RNA Folding and Catalysis Mediated by Iron (II)

Shreyas S. Athavale[1,3], Anton S. Petrov[1,3], Chiaolong Hsiao[2,3], Derrick Watkins[2,3], Caitlin D. Prickett[2,3], J. Jared Gossett[1,3], Lively Lie[1,3], Jessica C. Bowman[2,3], Eric O'Neill[2,3], Chad R. Bernier[2,3], Nicholas V. Hud[2,3], Roger M. Wartell[1,2], Stephen C. Harvey[1,2,3], Loren Dean Williams[2,3]*

1 School of Biology, Georgia Institute of Technology, Atlanta, Georgia, United States of America, 2 School of Chemistry and Biochemistry, Georgia Institute of Technology, Atlanta, Georgia, United States of America, 3 NAI Center for Ribosomal Origins and Evolution, Georgia Institute of Technology, Atlanta, Georgia, United States of America

Abstract

Mg^{2+} shares a distinctive relationship with RNA, playing important and specific roles in the folding and function of essentially all large RNAs. Here we use theory and experiment to evaluate Fe^{2+} in the absence of free oxygen as a replacement for Mg^{2+} in RNA folding and catalysis. We describe both quantum mechanical calculations and experiments that suggest that the roles of Mg^{2+} in RNA folding and function can indeed be served by Fe^{2+}. The results of quantum mechanical calculations show that the geometry of coordination of Fe^{2+} by RNA phosphates is similar to that of Mg^{2+}. Chemical footprinting experiments suggest that the conformation of the *Tetrahymena thermophila* Group I intron P4–P6 domain RNA is conserved between complexes with Fe^{2+} or Mg^{2+}. The catalytic activities of both the L1 ribozyme ligase, obtained previously by *in vitro* selection in the presence of Mg^{2+}, and the hammerhead ribozyme are enhanced in the presence of Fe^{2+} compared to Mg^{2+}. All chemical footprinting and ribozyme assays in the presence of Fe^{2+} were performed under anaerobic conditions. The primary motivation of this work is to understand RNA in plausible early earth conditions. Life originated during the early Archean Eon, characterized by a non-oxidative atmosphere and abundant soluble Fe^{2+}. The combined biochemical and paleogeological data are consistent with a role for Fe^{2+} in an RNA World. RNA and Fe^{2+} could, in principle, support an array of RNA structures and catalytic functions more diverse than RNA with Mg^{2+} alone.

Introduction

When large RNAs fold into compact structures, negatively charged phosphate groups achieve close proximity. Folded RNAs are stabilized in part by inorganic cations that accumulate in and around the RNA envelope. 'Diffuse' cations remain hydrated and make primary contributions to global stability by mitigating electrostatic repulsion of the negatively charged backbone. Chelated ions are less frequent, but in some instances are essential for achieving specific local conformation of the RNA. A special importance of Mg^{2+} in tRNA folding was seen early on [1–3]. It is now known that Mg^{2+} plays important roles in folding of essentially all large RNAs [4–6]. In addition, Mg^{2+} ions assist directly in stabilizing transition states of some ribozymes [7,8].

Here we use computation and experiment to address the question of whether Fe^{2+} can substitute for Mg^{2+} in RNA folding and catalysis. Mg^{2+} possesses important electronic and geometric properties that are key to its relationships with RNA. It is redox inactive, and does not cleave RNA via Fenton chemistry. The ionic radius of Mg^{2+} is small, the charge density is high, the coordination geometry is strictly octahedral, and the hydration enthalpy is large and negative [9–11]. In comparison with Group I cations, calcium, or polyamines, Mg^{2+} has a greater affinity for phosphate oxygens [12]. We find that Fe^{2+} is an excellent Mg^{2+} mimic in the absence of O_2, readily substituting for Mg^{2+} in RNA folding and catalysis.

Our primary motivation is to study RNA under plausible early earth conditions. Understanding the influence of Fe^{2+} on RNA structure and function could provide important links between the geological record and the RNA world. It is believed that life originated with RNA-based genetic and metabolic systems, i.e. the RNA world [13], which apparently flourished in an anoxic environment in which iron was much more soluble and abundant than in our current oxidative environment. Life evolved for around a billion years before the rise of photosynthesis and the Great Oxidation Event [14,15]. Fe^{2+}, either instead of or in combination with Mg^{2+}, seems to be a possible partner of RNA in the biology of the pre-photosynthesis anoxic earth.

With the rise in free oxygen, a product of photosynthesis, the Fe^{2+} of the early earth was oxidized and sequestered. Iron was deposited in banded iron formations (BIFs) [16], but BIF iron is seen by isotopic variations to have been a participant in ancient biological processes [17]. The transition from soluble to insoluble iron caused slow but dramatic shifts in biology and geology.

Results

Theory predicts that RNA conformation is conserved if Fe^{2+} substitutes for site-bound Mg^{2+}

Quantum mechanical (QM) calculations show that RNA conformation and coordination geometry are conserved when Mg^{2+} is replaced by Fe^{2+} in first shell RNA-metal complexes. We

focused here on an RNA-Mg^{2+} clamp [18], in which two adjacent RNA phosphates coordinate a common Mg^{2+} (Figure 1A). A complex with multiple first-shell RNA interactions with Mg^{2+} should provide a stringent test of the ability of Fe^{2+} to substitute. RNA-Mg^{2+} clamps are common in large RNAs [19]. One observes twenty-five RNA-Mg^{2+} clamps in the *Haloarcula marisortui* large ribosomal subunit [20], two in the P4-P6 domain of the *Tetrahymena thermophila* Group 1 intron [21], one in a self-splicing group II intron from *Oceanobacillus iheyensis* [22], and one in the L1 ribozyme ligase [23]. The folding and function of each of these RNAs is Mg^{2+} dependent.

The conformations of an RNA-Mg^{2+} clamp and an RNA-Fe^{2+} clamp are nearly identical, as determined by Density Functional Theory (DFT) [24]. The RNA conformation and metal-oxygen distances and angles are very similar (Figures 1B and 1C). The calculations do indicate some subtle differences, however. Calculated interaction energies (energies of complex formation, Table S1) favor Fe^{2+} over Mg^{2+} by 1.3 kcal/mol in continuum solvent as indicated by DFT calculations. Natural Bond Orbital analysis [25] in the gas phase (Table S2) suggests that more charge is transferred from phosphate to Fe^{2+} (0.43 e-) than from phosphate to Mg^{2+} (0.29 e-). This difference implies that compared to Mg^{2+}, Fe^{2+} better activates the phosphorous of RNA to nucleophilic attack. The increase in activation is attributable to the accessibility of the d-orbitals of Fe^{2+}.

Chemical probing suggests that RNA conformation is conserved when Fe^{2+} substitutes for Mg^{2+}

Selective 2′-hydroxyl acylation analyzed by primer extension (SHAPE) is a powerful RNA foot-printing technique that provides structural information at single-nucleotide resolution [26–28]. SHAPE has been used to accurately predict and confirm secondary structures of RNA ranging in length from tRNA to the HIV-1 genome [27,29]. The method exploits the reactivity of the 2′-hydroxyl groups of RNA to electrophiles to form 2′-O-ribose adducts. Here we employed the SHAPE reagent benzoyl cyanide (BzCN). The relative reactivities of ribose 2′-hydroxyl groups to the electrophile are sensitive to local RNA flexibility, which depends primarily on whether or not a nucleotide is base-paired. Single-stranded nucleotides react preferentially over double-stranded nucleotides. Reverse transcription using fluores-

cently labeled primers gives products that are truncated at locations indicating 2′-O-ribose adducts. The fragments are resolved and visualized using capillary electrophoresis. Capillary electrophoresis data were processed as described [30].

The secondary structure of the *T. thermophila* Group I intron P4–P6 domain was assayed by SHAPE in the presence of Na^+ alone, giving a reaction pattern consistent with the known secondary structure [21] (Figure 2A). For example, in the stem-loop formed by residues 143–160, the double-stranded nucleotides of the stem are unreactive while the GAAA nucleotides of the loop are reactive. Some of the most reactive nucleotides of the P4–P6 domain secondary structure are located within the A-rich bulge (nucleotides 182–188).

We probed the structure of the P4–P6 domain RNA in presence of Mg^{2+} (Figure 2B). The folding of RNAs from secondary structure to compact native states, containing long-range tertiary interactions, is known to be Mg^{2+}-dependent [4–6]. The addition of 2.5 mM Mg^{2+} to the P4–P6 domain RNA causes pronounced changes in the SHAPE reactivity. SHAPE reactivity increases at nucleotides 122, 125, 177–179 and 198–200 (indicated by asterisks in Figure 2B). The Mg^{2+}-dependence of SHAPE reactivities reflects (i) specific magnesium binding, (ii) diffuse interactions of Mg^{2+}, and (iii) RNA-RNA tertiary interactions facilitated by Mg^{2+}, as previously demonstrated for tRNA [27], RNase P [31], and Domain III of the ribosomal large subunit [30]. The pattern of SHAPE reactivity for P4–P6 domain RNA in the presence of Mg^{2+} observed here is nearly identical to that described previously for the same RNA in the presence of Mg^{2+} by Cech and coworkers (using N-methylisatoic anhydride instead of BzCN) [32].

The pattern of SHAPE reactivity for P4–P6 domain RNA is conserved when Mg^{2+} is replaced by Fe^{2+} under anaerobic conditions. Figure 2C shows that SHAPE reactivities in presence of 2.5 mM Fe^{2+} are identical, within the accuracy of the experiment, to those in presence of 2.5 mM Mg^{2+}. These results suggest that tertiary interactions and even the 'ion core' of the P4–P6 domain are recapitulated by Fe^{2+} in the absence of oxygen. As expected, if Fe^{2+} is added to the RNA in the presence of atmospheric free oxygen, the RNA is quickly degraded (not shown).
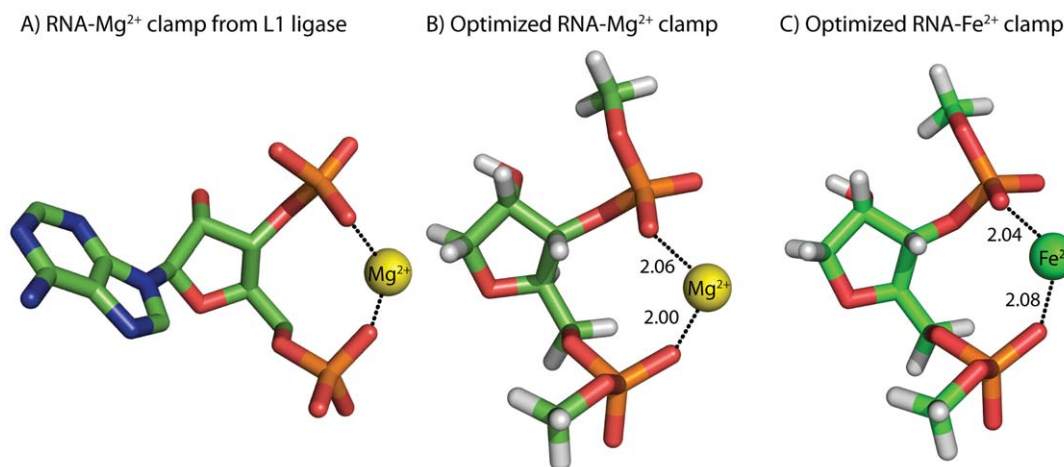

A) RNA-Mg^{2+} clamp from L1 ligase   B) Optimized RNA-Mg^{2+} clamp   C) Optimized RNA-Fe^{2+} clamp

Figure 1. Conformations of RNA-Mg^{2+} and RNA-Fe^{2+} clamps are nearly identical. A) RNA-Mg^{2+} clamp from the L1 ribozyme ligase (PDB 2OIU). B) RNA-Mg^{2+} clamp optimized by high level QM calculations. C) An optimized RNA-Fe^{2+} clamp. Each cation (Mg^{2+} or Fe^{2+}) is hexacoordinate. Mg^{2+} is shown as a yellow sphere and Fe^{2+} is shown as a green sphere. Water molecules are omitted from the images for clarity. Distances are in Å.
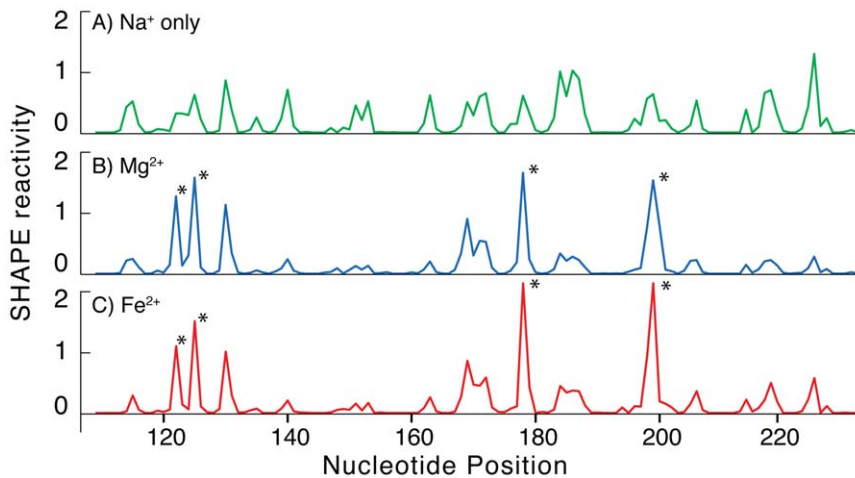doi:10.1371/journal.pone.0038024.g001

Figure 2. Addition of Mg^{2+} or Fe^{2+} causes the same changes in the SHAPE reactivity of the P4–P6 domain of the *T. thermophila* **Group 1 intron.** A) Shape profile in presence of 250 mM NaCl and no divalent cations. B) The addition of Mg^{2+} increases the reactivity at the sites indicated with the asterisks and decreases reactivity at other sites. This reaction contains 2.5 mM Mg^{2+} and 250 mM NaCl. C) The addition of Fe^{2+} causes the same changes in SHAPE reactivity as Mg^{2+}. This reaction contains 2.5 mM Fe^{2+} and 250 mM NaCl.
doi:10.1371/journal.pone.0038024.g002

Activity of two ribozymes is enhanced by Fe^{2+} compared to Mg^{2+}

To investigate RNA function in presence of Fe^{2+}, we tested the catalytic activity of the L1 ribozyme ligase in the presence of Mg^{2+} or Fe^{2+} (in the absence of oxygen). This ligase catalyzes formation of a phosphodiester linkage. The 3′-hydroxyl group of an RNA substrate attacks the α-phosphorus of the ribozyme 5′-triphosphate [23]. This ribozyme was selected *in vitro* in the presence of high [Mg^{2+}] (60 mM) by Robertson and Ellington, and has been described as Mg^{2+}-dependent [23]. The initial rate of ligation in 100 μM Mg^{2+} is 1.4×10^{-6} min^{-1}, while the initial rate of ligation in 100 μM Fe^{2+} is 3.5×10^{-5} min^{-1}, which is 25-fold higher (Figure 3A). A higher rate for Fe^{2+} over Mg^{2+} holds for essentially any reasonable equimolar concentration of the two cations. Achieving an equivalent rate of reaction requires around a 10-fold greater [Mg^{2+}] than [Fe^{2+}]. As expected, this ligase is inactive in Na$^+$ alone. This control, along with the chemical footprinting of the P4–P6 domain in Na$^+$ alone (Figure 2A), confirms the efficacy of our divalent cation extraction procedure using divalent cation chelating beads.

The hammerhead ribozyme was also assayed for activity in the presence of Fe^{2+}. Hammerhead ribozyme sequences are widely distributed in the tree of life [33]. This ribozyme cleaves the RNA backbone via nucleophilic attack by a 2′-hydroxyl group on the 3′-phosphorous atom [34]. In these reactions the initial rate of hammerhead cleavage in 25 μM Mg^{2+} is 0.011 min^{-1}, while the initial rate of cleavage in 25 μM Fe^{2+} is 0.035 min^{-1}, which is 3-fold higher (Figure 3B). The maximum fraction of cleaved substrate was about 3-fold greater in Fe^{2+} versus Mg^{2+}. When 100 μM of these two divalent cations were employed, Fe^{2+} again showed a higher initial rate of cleavage of ~3.5 fold (data not shown).

Discussion

The results here support a model of early evolution in which Fe^{2+} was an important metallo-cofactor for RNA. In this model, Fe^{2+} was replaced over time by Mg^{2+}, by processes driven at least in part by photosynthesis and the Great Oxidation Event.

The RNA World – on Steroids

The RNA world is hypothesized to have occurred during the early Archean eon, prior to the Great Oxidation Event. Fe^{2+} in the early Archean would have been available, soluble and non-toxic. Our observations here of Fe^{2+}-mediated RNA folding and catalysis, in combination with paleogeological information, suggest that RNA could have originated and evolved in association with Fe^{2+}. The RNA-Fe^{2+} complexes recently observed in extant biology [35] could be molecular fossils from the RNA world, akin to the ribosome. The injection of Fe^{2+} into RNA World models opens broad new possibilities for ancient biochemistry. RNA and Fe^{2+} could, in principle, support an array of RNA structures and catalytic functions far more diverse than RNA with Mg^{2+} alone. Complexes of RNA with Fe^{2+} offer the prospect of redox chemistry and electron transfer reactions for ancient ribozymes.

Replacement of Fe^{2+} by Mg^{2+} in RNA is analogous to replacement of Fe^{2+} by Mn^{2+} in protein enzymes

The conversion of one metal to another is facile in some protein enzymes. In just one example, Mn^{2+} and Fe^{2+} are used as cofactors in a broad class of superoxide dismutases (Fe^{2+}/Mn^{2+} SODs) [36]. The metal cofactors of these SODs can be interconverted between Mn^{2+} and Fe^{2+} while the coordination geometry, amino acid sequence and global fold of the protein are conserved. The discrimination between Fe^{2+} and Mn^{2+} in Fe^{2+}/Mn^{2+} SODs *in vivo* is determined by species, organelle, protein isozyme, protein expression level and metal bioavailability. Metal substitution appears to be a useful biological strategy in nutrient-limited environments [37–39]. Falkowski has proposed that during the Great Oxidation Event, Mn^{2+} was appropriated into some Fe^{2+} dependent enzymes [37]. Here we suggest that the same strategy was employed with RNA, where Fe^{2+} was converted to Mg^{2+}. It has been suggested, based on sites of Fenton cleavage (using iron/ O$_2$), that Fe^{2+} and Mg^{2+} compete for common sites in RNA [40–42] *in vitro*.
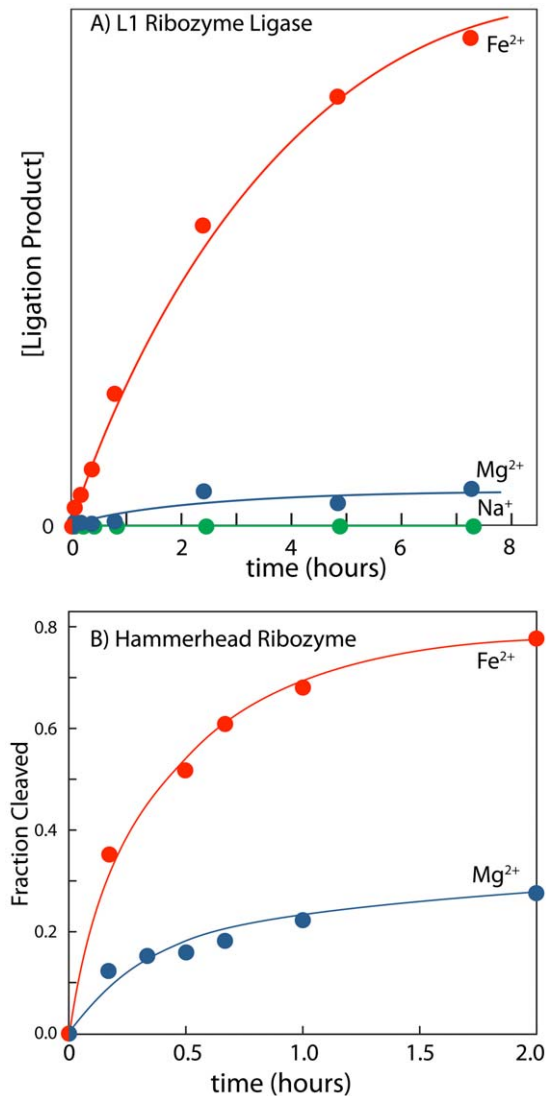
Figure 3. Ribozyme activity is enhanced by Fe²⁺ compared to Mg²⁺. A) L1 ribozyme ligase activity is enhanced in Fe²⁺ compared to Mg²⁺. Ligase reactions were performed under anaerobic conditions at room temperature and 250 mM Na⁺ in 100 μM [Fe²⁺] or 100 μM [Mg²⁺]. The reaction components were first annealed in 50 mM HEPES, pH 8.0, 200 mM sodium acetate by incubating at 90°C for 3 min and cooling to room temperature over 30 min. The ligation reaction was initiated by adding the appropriate cation salt. The Na⁺ only reaction gave no product. Reaction progress was monitored by gel electrophoresis. B) Hammerhead ribozyme activity is enhanced in Fe²⁺ compared to Mg²⁺. Hammerhead ribozyme cleavage reactions were performed under anaerobic conditions at room temperature in 50 mM HEPES, pH 7.5 and 25 μM [Fe²⁺] or 25 μM [Mg²⁺]. Substrate and ribozyme RNA strands were first annealed in 50 mM HEPES buffer by incubating at 90°C for 2 min and cooling to room temperature over 30 min. Cleavage reactions were initiated by addition of FeCl₂ or MgCl₂ from stock solutions. Reactions were monitored by both gel electrophoresis and capillary electrophoresis, which gave similar results.
doi:10.1371/journal.pone.0038024.g003

QM calculations suggest that an RNA fragment that forms multiple first-shell interactions with Mg²⁺ does not change conformation when Mg² is replaced by Fe²⁺

The metal-oxygen distances and angles are nearly identical in the Mg²⁺ and Fe²⁺ complexes (Figures 1B and 1C). The QM

calculations do indicate subtle differences between Mg²⁺ and Fe²⁺ complexes. It appears that more charge is transferred from phosphate to Fe²⁺ than from phosphate to Mg²⁺. This electronic difference, which activates the phosphorus atom to nucleophilic attack, is attributable to the accessibility of the d-orbitals of Fe²⁺.

Chemical probing experiments in solution, using the T. thermophila Group I intron P4–P6 domain RNA, demonstrate the ability of Fe²⁺ to substitute for Mg²⁺ during folding of large RNAs

The P4–P6 domain interacts with Mg²⁺ by a complex blend of diffuse and chelated modes [21,43,44]. In spite of this complexity, the changes in SHAPE reactivity of RNA induced by association with Mg²⁺ or Fe²⁺ in the absence of free oxygen are very similar (Figures 2B and 2C). SHAPE reports local RNA flexibility, which depends primarily on whether or not a nucleotide is base-paired in secondary or tertiary interactions. The results for the P4–P6 domain suggest that in the absence of free oxygen, Fe²⁺ can replace Mg²⁺ in compacting and folding large RNAs. Thus it appears that Fe²⁺ and Mg²⁺ are nearly interchangeable in their interactions with RNA.

Fe²⁺ can substitute for Mg²⁺ to support catalysis by ribozymes

At equimolar concentrations of Mg²⁺ or Fe²⁺, the initial rate of ligation observed for the L1 ribozyme ligase is 25-fold higher with Fe²⁺ than Mg²⁺ in the absence of free oxygen (Figure 3A). Similarly, at equimolar concentrations of Mg²⁺ or Fe²⁺, the initial rate of RNA cleavage observed for the hammerhead ribozyme is 3-fold higher with Fe²⁺ than Mg²⁺ (Figure 3B). In sum, we have looked at RNA folding in three independent experimental systems, by chemical footprinting (P4–P6 domain), and with two ribozyme assays (L1 ribozyme ligase and the hammerhead ribozyme). In each system examined, Fe²⁺ substitutes for Mg²⁺ in the absence of free oxygen. The increased activities of the ribozymes with Fe²⁺ over Mg²⁺ are consistent with our computational results that suggest Fe²⁺ is slightly better than Mg²⁺ at activating the phosphorous of RNA to nucleophilic attack. In the hammerhead, which is one of the best-characterized ribozymes, it has been shown that a Mg²⁺ ion interacts directly with the scissile phosphate before and during catalysis [45]. The results here suggest that Fe²⁺ is a superior substitute for Mg²⁺ in this catalytic role. A variety of effects such as differential affinity of Fe²⁺ and Mg²⁺ globally, or for various sites on RNA, could also contribute to differences in cleavage rates.

How much Fe²⁺ was available during the time of the RNA World?

It seems very likely that the early Archean earth provided a variety of Fe²⁺-rich microenvironments. On a global scale, the [Fe²⁺]$_{marine}$ in the early Archean is subject to debate, and is largely circumscribed in current models by P$_{CO2}$ (atmospheric pressure of CO₂) in the atmosphere (Fe²⁺ precipitates as siderite: Fe²⁺CO₃⁻). Early earth P$_{CO2}$ is inferred using estimates of greenhouse effects, sun luminosity, earth albedo and temperatures required to maintain liquid oceans. A variety of recent results challenge high P$_{CO2}$ models [46,47]. If P$_{CO2}$ was low, [Fe²⁺]$_{marine}$ could have been as high as 100–1000 μM [14,48], compared to 0.3–0.8 nM in the modern ocean [49]. P$_{HS}$ (atmospheric pressure of HS) would also have been an important influence on [Fe²⁺]$_{marine}$ due to precipitation of FeS [50].

How much Mg^{2+} was available during the RNA World?

The $[Mg^{2+}]_{marine}$ in the early Archean is also uncertain. Although the models are tentative, it has been suggested that $[Mg^{2+}]_{marine}$ during this time was attenuated by submarine hydrothermal systems associated with higher heat flow [51,52], more vigorous seafloor spreading [53,54], and by reduced Mg^{2+} delivery to the oceans by smaller continental landmasses or from the weathering of peridotite in the sea floor [55]. Both of these phenomena would tend to lower $[Mg^{+2}]_{marine}$ of early oceans in comparison to today.
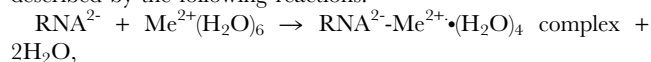
Fe^{2+} is the double-edged sword

The early earth's abundant Fe^{2+} has been oxidized and sequestered to the extent that current biomass and species diversity in many ecosystems is limited by Fe^{2+} availability [56,57]. Iron in the presence of oxygen is rare, toxic, and biologically expensive to manage [58,59]. Yet living systems are dependent on and must acquire and utilize iron. The concentration of iron in cells is on the order of 100 µM, with iron largely constrained to heme, iron-sulfur clusters, and di-iron or mono-iron centers, transporters, carriers, exporters, and concentrators such as ferritins [60]. Because the solubility of ferric iron in water or plasma is so low (10^{-18} M), cells must combat a massive concentration gradient. The transition from benign and abundant iron to scarce and toxic iron would have caused a slow but dramatic shift in biology that required transformations in biochemical mechanisms and metabolic pathways.

Materials and Methods

QM calculations

The initial atomic coordinates of a Mg^{2+}-RNA clamp were extracted from the X-ray structure of the *H. marismortui* large ribosomal subunit (PDB entry 1JJ2) [20] as previously described [19]. The 5′ and 3′ phosphates were capped with methyl groups in lieu of the remainder of the RNA polymer and hydrogen atoms were added, where appropriate. The Fe^{2+}-RNA clamp was constructed by replacing the magnesium ion with an iron as described [18].

The binding of a Mg^{2+} or Fe^{2+} ion to an RNA fragment was described by the following reactions:

$$RNA^{2-} + Me^{2+}(H_2O)_6 \rightarrow RNA^{2-}\text{-}Me^{2+}\cdot(H_2O)_4 \text{ complex} + 2H_2O,$$

where $Me^{2+} = (Mg^{2+}, Fe^{2+})$

The reactants and products were fully optimized using density functional theory (DFT) at the B3LYP level, which combines the GGA exchange three-parameter hybrid functional developed by Becke [61] and the correlation functional of Lee-Yang-Parr [62] and the $6\text{--}311G(d,p)^{++}$ basis set and multiplicity = 1 as implemented in Gaussian 09 [63]. The Fe^{2+}-RNA clamp and the $Fe^{2+}(H_2O)_6$ were optimized at the unrestricted B3LYP/6–31G(d,p) level of theory with spin of iron = 2 and multiplicity = 5. Single point energies for these complexes were further obtained at the UB3LYP/6–311++G(d,p) level of theory using SCF options DIIS, NOVARACC, VTL, MaxCyc = 1000.

The interaction energies were calculated in water using the gas phase optimized geometries within the framework of the Integral Equation Formalism of Polarized Continuum Model [24]. The basis set superposition error (BSSE) in the dimer-centered basis set was obtained by applying the counterpoise procedure of Boys and Bernardi [64]. The corrected interaction energies were calculated by taking into account deformational energies of monomers according to the scheme proposed by van Duijneveldt-van de

Rijdt and van Duijneveldt [65]. The IEFPCM approach was used to account for the effect of a polar solvent.

Natural Bond Order (NBO) [25] and Natural Energy Decomposition Analysis (NEDA) [66,67] calculations were performed on the optimized complexes at the (U)B3LYP/6–31G(d,p) level of theory using the GAMESS package [68].

DNA and RNA synthesis

The genes and RNA transcripts for the L1 ribozyme ligase and the P4–P6 domain the *Tetrahymena thermophila* Group 1 intron were synthesized and purified as described in Text S1. After transcription, Mg^{2+} was removed from the RNA by heat annealing in the presence of divalent cation chelating beads (Hampton Research). SHAPE reactivity and ribozyme reactions confirm that the divalent cations are removed by chelating beads.

SHAPE probing of P4–P6 RNA

All manipulations of RNA with Fe^{2+} were conducted in a Coy chamber with an atmosphere of 85% N_2, 10% CO_2, 5% H_2. P4–P6 domain RNA (11.25 µg) was lyophilized, transferred to the anaerobic chamber, left open for several hours, and resuspended in 240 µL of 50 mM HEPES, pH 8.0, 200 mM sodium acetate (final concentration) that had been previously deoxygenated by bubbling with argon for several hours. The RNA was denatured and renatured using a thermal cycler, by heating to 90°C for 3 min and then quickly cooling to 4°C. Eighty µL of the RNA solution was aliquoted into three tubes. To the first tube, 10 µL of 25 mM $FeCl_2$ (Avantor Performance Materials) solution was added. To the second tube, 10 µL of 25 mM $MgCl_2$ was added. To the third tube, 10 µL water was added. The tubes were incubated at room temperature for 5 minutes. The RNA from each tube was then divided equally between two additional tubes. To one tube of each pair, 5 µL of 800 mM benzoyl cyanide (BzCN) in anhydrous DMSO was added. The other tube of the pair served as a negative control, to which 5 µL neat DMSO was added. The benzoyl cyanide reactions are complete in a few seconds at room temperature [31]. The Fe^{2+} was removed by treatment with chelating beads. The beads and the associated divalent cations were removed with a 0.2 micron filtration spin column. Denaturing SHAPE experiments were performed in 20 mM HEPES pH 8.0 (final concentration) for 4 min at 90°C using 130 mM *N*-methylisatoic anhydride (NMIA) in anhydrous DMSO. Modified RNA was purified using RNeasy Mini Kit (Qiagen) and re-suspended in 20 µL 1× TE. The recovery after purification was 65–75%.

A 20-nt long DNA oligomer, 5′- GAACTGCATCCATAT-CAACA -3′, that anneals to the 3′-end of the P4-P6 domain, was used to prime reverse transcription. The primer was labeled with 6-FAM at its 5′-end (Eurofins MWG Operon). Reverse transcription, capillary electrophoresis and data processing were performed as described [30].

L1 ribozyme ligation reactions

As noted above, all manipulations in which RNA was in contact with Fe^{2+} were conducted in a Coy chamber. The substrate RNA (5′-UGCACU-3′) labeled with Cy3 at its 5′-end and DNA enhancer (5′-GCGACTGGACATCACGAG-3′) were purchased from Eurofins MWG Operon. Aliquoted reaction components (L1 ligase RNA, substrate RNA and DNA enhancer; typical molar ratio used was 1:0.1:2, respectively) were lyophilized separately, transferred to the anaerobic chamber, left open for several hours, and resuspended in 50 mM HEPES, pH 8.0, 200 mM sodium acetate that had been previously deoxygenated by bubbling with argon for several hours. The reaction components were annealed

inside the anaerobic chamber by incubating at 90°C for 3 min and cooling to room temperature over 30 min. FeCl$_2$ was weighed and dissolved in water inside the anaerobic chamber. The final volumes of the reaction mixtures were generally 270 µL.

Ligation reactions were initiated by addition of the appropriate cation salt to the dissolved reaction components. At predetermined time points, 30 µL aliquots were withdrawn and quenched by treatment with chelating beads. The beads and divalent cations were removed with a spin column and the samples were frozen and stored at −80°C. The L1 ligase RNA was stable for days in 10 mM Fe^{2+} in the anaerobic chamber, but degraded quickly upon exposure to atmospheric oxygen. After the Fe^{2+} was removed with chelating beads, the L1 ligase RNA was stable to exposure to atmospheric oxygen.

For gel analysis, 5 µL of reaction mixture was mixed with 15 µL loading buffer (8 M urea, 1× TTE, 10% glycerol) and denatured by heating to 90°C for 2 min. The reaction components were then resolved on 8% denaturing PAGE gels and visualized on a Typhoon Trio variable mode imager. Some representative gels are shown in Figure S1. The band intensities were quantified using Fujifilm MultiGauge 2.0 software.

Hammerhead ribozyme cleavage reactions

As noted above, all manipulations of the hammerhead RNA in the presence of Fe^{2+} were carried out in a Coy chamber. The hammerhead ribozyme-substrate was based on the unmodified HHα1 RNA described by Stage-Zimmermann and Uhlenbeck [69]. A 31 nucleotide substrate strand (5′-GGCAAUC-GAAACGCGAAAGCGUCUAGCGGGC-3′), labeled at the 3′-end with FAM, and the 21 nucleotide ribozyme strand (5′-CCCGCUACUGAUGAGAUUGCC-3′) were purchased from IDT. Substrate and ribozyme strands (typical molar ratio used was 1:1000) were lyophilized separately, transferred to the anaerobic chamber, left open for several hours, and resuspended in 50 mM HEPES, pH 7.5 (pH adjusted with KOH). The buffer had previously been deoxygenated by bubbling with argon for several hours. The strands were annealed inside the anaerobic chamber by incubating at 90°C for 2 min and cooling to room temperature over 30 min.

Reactions (150 µL final volume) were initiated by addition of 1.5 µL of cation solution (Fe^{2+} or Mg^{2+}). At predetermined time points, 20 µL aliquots were withdrawn and quenched by treatment with divalent cation chelating beads. The beads and the associated divalent cations were removed with a spin column, and the samples were frozen and stored at −80°C. For gel analysis, 1 µL of reaction mixture was mixed with 9 µL loading

buffer (8 M urea, 1× TTE, 10% glycerol) and denatured by heating to 90°C for 2 minutes. The intact 31 nucleotide substrate and 7 nucleotide product were resolved on 15% denaturing PAGE gels and visualized on a Typhoon Trio variable mode imager, or separated by capillary electrophoresis and quantified as described previously [30].

Supporting Information

Figure S1 8% polyacrylamide – 8 M urea denaturing gels showing L1 Ribozyme Ligase reaction progress. Only species tagged with 5′-Cy3 dye (substrate and product) are visible. The L1 Ribozyme Ligase is visible when the gel is stained with cyber gold or ethidium. The reaction rate increases when [Fe^{2+}] is increased from 100 µM (LH panel, reaction product observable at 4 hours) to 625 µM (center panel, reaction product observable at first time point, 30 min). The rate of the reaction in 1 mM Mg^{2+} (RH panel) is roughly equivalent to that in 100 µM Fe^{2+} (LH panel).
(TIF)

Table S1 Electronic energies, interaction energies and the corresponding counterpoise-corrected interaction energies calculated at the (U)B3LYP/6–311++G(d,p) level of theory within the framework of IEFPCM in water.
(DOCX)

Table S2 Electronic configurations of Mg^{2+} and Fe^{2+} in the RNA^{2-}-Mg^{2+}(H$_2$O)$_4$ and RNA^{2-}-Fe^{2+}(H$_2$O)$_4$ complexes as revealed by the NBO at the (U)B3LYP/6–31G(d,p) level of theory.
(DOCX)

Text S1 RNA Synthesis and Purification.
(DOCX)

Acknowledgments

Author Contributions

Conceived and designed the experiments: SSA ASP CH DW CDP LL RMW SCH NVH LDW. Performed the experiments: SSA ASP DW CDP LL. Analyzed the data: SSA ASP DW CDP LL JJG NVH SCH RMW LDW. Contributed reagents/materials/analysis tools: JCB EO CRB JJG. Wrote the paper: SSA LDW ASP RMW NVH SCH.

References

1. Stein A, Crothers DM (1976) Conformational changes of transfer RNA. The role of magnesium (II) equilibrium binding of magnesium (II) by Escherichia coli tRNA^{fMet}. Biochemistry 15: 160–168.
2. Lynch DC, Schimmel PR (1974) Cooperative binding of magnesium to transfer ribonucleic acid studied by a fluorescent probe. Biochemistry 13: 1841–1852.
3. Lindahl T, Adams A, Fresco JR (1966) Renaturation of transfer ribonucleic acids through site binding of magnesium. Proc Natl Acad Sci U S A 55: 941–948.
4. Brion P, Westhof E (1997) Hierarchy and dynamics of RNA folding. Annu Rev Biophys Biomol Struct 26: 113–137.
5. Draper DE (2008) RNA folding: Thermodynamic and molecular descriptions of the roles of ions. Biophys J 95: 5489–5495.
6. Auffinger P, Grover N, Westhof E (2011) Metal ion binding to RNA. Met Ions Life Sci 9: 1–35.
7. Butcher SE (2011) The spliceosome and its metal ions. Met Ions Life Sci 9: 235–251.
8. Johnson-Buck AE, McDowell SE, Walter NG (2011) Metal ions: Supporting actors in the playbook of small ribozymes. Met Ions Life Sci 9: 175–196.
9. Brown ID (1992) Chemical and steric constraints in inorganic solids. Acta Crystallogr Sect B 48: 553–572.
10. Rashin AA, Honig B (1985) Reevaluation of the Born model of ion hydration. J Phys Chem 89: 5588–5593.
11. Bock CW, Markham GD, Katz AK, Glusker JP (2006) The arrangement of first- and second-shell water molecules around metal ions: Effects of charge and size. Theor Chem Acc 115: 100–112.
12. Hsiao C, Tannenbaum M, VanDeusen H, Hershkovitz E, Perng G, Tannenbaum A, Williams LD (2008) Complexes of nucleic acids with group I and II cations. Hud N, editor. Nucleic acid metal ion interactions. London: The Royal Society of Chemistry. pp 1–35.
13. RNA worlds: From life's origins to diversity in gene regulation (2011) Atkins JF, Gesteland RF, Cech TR, editors: Cold Spring Harbor Laboratory Press.
14. Anbar AD (2008) Oceans. Elements and evolution. Science 322: 1481–1483.
15. Hazen RM, Ferry JM (2010) Mineral evolution: Mineralogy in the fourth dimension. Elements 6: 9–12.
16. Klein C (2005) Some Precambrian banded iron-formations (BIFs) from around the world: Their age, geologic setting, mineralogy, metamorphism, geochemistry, and origin. Am Mineral 90: 1473–1499.
17. Johnson CM, Beard BL, Roden EE (2008) The iron isotope fingerprints of redox and biogeochemical cycling in modern and ancient earth. Annual Review of Earth and Planetary Sciences 36: 457–493.

18. Petrov AS, Bowman JC, Harvey SC, Williams LD (2011) Bidentate RNA-magnesium clamps: On the origin of the special role of magnesium in RNA folding. RNA 17: 291–297.

19. Hsiao C, Williams LD (2009) A recurrent magnesium-binding motif provides a framework for the ribosomal peptidyl transferase center. Nucleic Acids Res 37: 3134–3142.

20. Ban N, Nissen P, Hansen J, Moore PB, Steitz TA (2000) The complete atomic structure of the large ribosomal subunit at 2.4 Å resolution. Science 289: 905–920.

21. Cate JH, Hanna RL, Doudna JA (1997) A magnesium ion core at the heart of a ribozyme domain. Nat Struct Biol 4: 553–558.

22. Toor N, Keating KS, Taylor SD, Pyle AM (2008) Crystal structure of a self-spliced group II intron. Science 320: 77–82.

23. Robertson MP, Scott WG (2007) The structural basis of ribozyme-catalyzed RNA assembly. Science 315: 1549–1553.

24. Tomasi J, Mennucci B, Cances E (1999) The IEF version of the PCM solvation method: An overview of a new method addressed to study molecular solutes at the QM ab initio level. Journal of Molecular Structure-Theochem 464: 211–226.

25. Glendening ED, Streitwieser A (1994) Natural energy decomposition analysis-an energy partitioning procedure for molecular-interactions with application to weak hydrogen-bonding, strong ionic, and moderate donor-acceptor interactions. J Chem Phys 100: 2900–2909.

26. Merino EJ, Wilkinson KA, Coughlan JL, Weeks KM (2005) RNA structure analysis at single nucleotide resolution by selective 2′-hydroxyl acylation and primer extension (SHAPE). J Am Chem Soc 127: 4223–4231.

27. Wilkinson KA, Merino EJ, Weeks KM (2005) RNA SHAPE chemistry reveals nonhierarchical interactions dominate equilibrium structural transitions in tRNA(asp) transcripts. J Am Chem Soc 127: 4659–4667.

28. Mortimer SA, Weeks KM (2007) A fast-acting reagent for accurate analysis of RNA secondary and tertiary structure by SHAPE chemistry. J Am Chem Soc 129: 4144–4145.

29. Wilkinson KA, Gorelick RJ, Vasa SM, Guex N, Rein A, Mathews DH, Giddings MC, Weeks KM (2008) High-throughput SHAPE analysis reveals structures in hiv-1 genomic RNA strongly conserved across distinct biological states. PLoS Biol 6: 883–899.

30. Athavale SS, Gossett JJ, Hsiao C, Bowman JC, O'Neill E, Hershkovitz E, Preeprem T, Hud NV, Wartell RM, Harvey SC, Williams LD (2012) Domain III of the *T. thermophilus* 23S rRNA folds independently to a near-native state. RNA 18: 752–758.

31. Mortimer SA, Weeks KM (2008) Time-resolved RNA SHAPE chemistry. J Am Chem Soc 130: 16178–16180.

32. Vicens Q, Gooding AR, Laederach A, Cech TR (2007) Local RNA structural changes induced by crystallization are revealed by SHAPE. RNA 13: 536–548.

33. Seehafer C, Kalweit A, Steger G, Graf S, Hammann C (2011) From alpaca to zebrafish: Hammerhead ribozymes wherever you look. RNA 17: 21–26.

34. Scott WG (2007) Ribozymes. Curr Opin Struct Biol 17: 280–286.

35. Goss DJ, Theil EC (2011) Iron responsive mRNAs: A family of Fe^{2+} sensitive riboregulators. Acc Chem Res 44: 1320–1328.

36. Aguirre JD, Culotta VC (2012) Battles with iron: Manganese in oxidative stress protection. J Biol Chem 287: 13541–13548.

37. Wolfe-Simon F, Starovoytov V, Reinfelder JR, Schofield O, Falkowski PG (2006) Localization and role of manganese superoxide dismutase in a marine diatom. Plant physiology 142: 1701–1709.

38. Peers G, Price NM (2004) A role for manganese in superoxide dismutases and growth of iron-deficient diatoms. Limnol Oceanogr 49: 1774–1783.

39. Whitfield M (2001) Interactions between phytoplankton and trace metals in the ocean. Adv Mar Biol: Academic Press. pp 1–128.

40. Vary CP, Vournakis JN (1984) RNA structure analysis using methidiumpropyl-EDTA-Fe(II): A base-pair-specific RNA structure probe. Proc Natl Acad Sci U S A 81: 6978–6982.

41. Hanson S, Bauer G, Fink B, Suess B (2005) Molecular analysis of a synthetic tetracycline-binding riboswitch. RNA 11: 503–511.

42. Wang JF, Cech TR (1992) Tertiary structure around the guanosine-binding site of the tetrahymena ribozyme. Science 256: 526–529.

43. Takamoto K, Das R, He Q, Doniach S, Brenowitz M, et al. (2004) Principles of RNA compaction: Insights from the equilibrium folding pathway of the P4–P6 RNA domain in monovalent cations. J Mol Biol 343: 1195–1206.

44. Misra VK, Draper DE (2001) A thermodynamic framework for Mg^{2+} binding to RNA. Proc Natl Acad Sci U S A 98: 12456–12461.

45. Ward WL, Derose VJ (2012) Ground-state coordination of a catalytic metal to the scissile phosphate of a tertiary-stabilized hammerhead ribozyme. RNA 18: 16–23.

46. Rosing MT, Bird DK, Sleep NH, Bjerrum CJ (2010) No climate paradox under the faint early sun. Nature 464: 744–747.

47. Som SM, Catling DC, Harnmeijer JP, Polivka PM, Buick R (2012) Air density 2.7 billion years ago limited to less than twice modern levels by fossil raindrop imprints. Nature 484: 359–362.

48. Holland H (1984) The chemical evolution of the atmosphere and oceans. Princeton, New Jersey: Princeton University Press. 582 p.

49. Moore JK, Braucher O (2007) Observations of dissolved iron concentrations in the world ocean: Implications and constraints for ocean biogeochemical models. Biogeosciences Discuss 4: 1241–1277.

50. Hazen RM, Papineau D, Bleeker W, Downs RT, Ferry JM, McCoy TJ, Sverjensky DA, Yang H (2008) Mineral evolution. Am Mineral 93: 1693–1720.

51. Condie KC (2007) The distribution of paleoarchean crust. Van Kranendonk MJ, Smithies RH, Bennett VC, editors. Earth's oldest rocks. Elsevier Publishers.

52. Tajika E, Matsui T (1992) Evolution of terrestrial proto-CO_2 atmosphere coupled with thermal history of the earth. Earth and Planetary Science Letters 113: 251–266.

53. Condie KC, Kroner A (2008) When did plate tectonics begin? Evidence from the geologic record. Condie KC, Pease V, editors. Geological society of America special papers. pp 281–294.

54. Davies GF (1992) On the emergence of plate-tectonics. Geology 20: 963–966.

55. Snow JE, Dick HJB (1995) Pervasive magnesium loss by marine weathering of peridotite. Geochim Cosmochim Acta 59: 4219–4235.

56. Sunda WG, Huntsman SA (1995) Iron uptake and growth limitation in oceanic and coastal phytoplankton. Mar Chem 50: 189–206.

57. Coale KH, Johnson KS, Fitzwater SE, Gordon RM, Tanner S, et al. (1996) A massive phytoplankton bloom induced by an ecosystem-scale iron fertilization experiment in the equatorial pacific ocean. Nature 383: 495–501.

58. Kell DB (2009) Iron behaving badly: Inappropriate iron chelation as a major contributor to the aetiology of vascular and other progressive inflammatory and degenerative diseases. BMC Med Genomics 2: 2.

59. Chiancone E, Ceci P, Ilari A, Ribacchi F, Stefanini S (2004) Iron and proteins for iron storage and detoxification. BioMetals 17: 197–202.

60. Theil EC, Goss DJ (2009) Living with iron (and oxygen): Questions and answers about iron homeostasis. Chem Rev 109: 4568–4579.

61. Becke AD (1988) Density-functional exchange-energy approximation with correct asymptotic behavior. Physical Review A 38: 3098–3100.

62. Lee CT, Yang WT, Parr RG (1988) Development of the Colle-Salvetti correlation energy formula into a functional of the electron density. Physical Review B 37: 785–789.

63. Frisch MJ, Trucks GW, Schlegel HB, Scuseria GE, Robb MA, et al. (2009) Gaussian 09, revision A.01. Wallingford, CT: Gaussian, Inc.

64. Boys SF, Bernardi F (1970) Calculation of small molecular interactions by differences of separate total energies-some procedures with reduced errors. Mol Phys 19: 553–566.

65. van Duijneveldt-van de Rijdt JGCM, van Duijneveldt FB (1997) Ab initio methods applied to hydrogen bonded systems. Hadzi D, editor. Theoretical treatments of hydrogen bonding. Chichester, UK: Wiley. pp 13–47.

66. Glendening ED (1996) Natural energy decomposition analysis: Explicit evaluation of electrostatic and polarization effects with application to aqueous clusters of alkali metal cations and neutrals. J Am Chem Soc 118: 2473–2482.

67. Schenter GK, Glendening ED (1996) Natural energy decomposition analysis: The linear response electrical self energy. J Phys Chem 100: 17152–17156.

68. Gordon MS, Schmidt MW (2005) Advances in electronic structure theory: Gamess a decade later. In: Dykstra CE, Frenking G, Kim KS, Scuseria GE, eds. Theory and applications of computational chemistry: The first forty years. Amsterdam: Elsevier.

69. Stage-Zimmermann TK, Uhlenbeck OC (2001) A covalent crosslink converts the hammerhead ribozyme from a ribonuclease to an RNA ligase. Nat Struct Biol 8: 863–867.